Biomaterials Advances 154 (2023) 213633

Contents lists available at ScienceDirect

Biomaterials Advances

journal homepage: www.journals.elsevier.com/materials-science-and-engineering-c

Host bone microstructure for enhanced resistance to bacterial infections

Ryota Watanabe [a,b], Aira Matsugaki [b], Ozkan Gokcekaya [b], Ryosuke Ozasa [b], Takuya Matsumoto [c], Hiroyuki Takahashi [a], Hidekazu Yasui [a], Takayoshi Nakano [b,*]

[a] Teijin Nakashima Medical Co. Ltd., 688-1 Joto-Kitagata, Higashi-ku, Okayama 709-0625, Japan
[b] Division of Materials and Manufacturing Science, Graduate School of Engineering, Osaka University, 2-1, Yamada-Oka, Suita, Osaka 565-0871, Japan
[c] Department of Biomaterials, Graduate School of Medicine, Dentistry and Pharmaceutical Sciences, Okayama University, 2-5-1, Shikata-cho, Kita-ku, Okayama 700-8558, Japan

ARTICLE INFO

Keywords:
Postoperative infection
Laser powder bed fusion
Titanium alloy
Surface topography
Bone matrix anisotropy
Antimicrobial activity

ABSTRACT

Postoperative bacterial infection is a serious complication of orthopedic surgery. Not only infections that develop in the first few weeks after surgery but also late infections that develop years after surgery are serious problems. However, the relationship between host bone and infection activation has not yet been explored. Here, we report a novel association between host bone collagen/apatite microstructure and bacterial infection. The bone-mimetic-oriented micro-organized matrix structure was obtained by prolonged controlled cell alignment using a grooved-structured biomedical titanium alloy. Surprisingly, we have discovered that highly aligned osteoblasts have a potent inhibitory effect on *Escherichia coli* adhesion. Additionally, the oriented collagen/apatite micro-organization of the bone matrix showed excellent antibacterial resistance against *Escherichia coli*. The proposed mechanism for realizing the antimicrobial activity of the micro-organized bone matrix is by the controlled secretion of the antimicrobial peptides, including β-defensin 2 and β-defensin 3, from the highly aligned osteoblasts. Our findings contribute to the development of anti-infective strategies for orthopedic surgeries. The recovery of the intrinsically ordered bone matrix organization provides superior antibacterial resistance after surgery.

1. Introduction

Postoperative infection is a serious complication of spinal surgery and total joint arthroplasty. Although the incidences of infection have been reported to be 0.58–1.60 % in total knee arthroplasty and <1–11 % in spinal surgery [1,2], postoperative infections may cause implant removal, increased morbidity, and possible mortality, and increase the economic and social costs [3–5]. Additionally, the number of surgeries performed in the United States is increasing [6,7] and the infection rate is predicted to increase. The rate of infection is also higher after revision surgery than after primary surgery [8–10]; thus, the number of infected patients also increases.

Although most cases of postoperative infections are reported within several weeks [11,12], late infections occurring after years are also problems. Most studies have suggested that the complete removal of implants is required to treat late infections [13,14]. Late infections have been reported to result in higher treatment failure rates [12]. Therefore, developing new antimicrobial implants is imperative to prevent late infections. Silver-containing hydroxyapatite coatings (Ag-HA) have been applied to orthopedic implants to prevent infections clinically [15]. Although the occurrence of postoperative infections in Ag-HA implants has been significantly reduced [16,17], *in vitro* studies have shown pronounced silver ion release for up to 24 h followed by the rates decreasing with time [18]. These findings indicate that the duration of the antimicrobial effects is not enough to tolerate long-term infection. It is worthy of note that current findings indicate novel coating methods for ion release using metal nanotubes [19–21] and ceramics coating [22,23] are effective for antimicrobial functions.

The "race for the surface" theory [24,25] has been widely recognized for preventing bacteria adhesion and biofilm formation on the implant surface. Briefly, if host cells first adhere to the implant surface, the surface is covered with cells, resulting in less bacterial colonization. However, if the bacteria win the race, the implant surface will be covered with a bacterial biofilm, leading to infection. This theory

* Corresponding author.
E-mail addresses: r.watanabe@teijin-nakashima.co.jp (R. Watanabe), matsugaki@mat.eng.osaka-u.ac.jp (A. Matsugaki), ozkan@mat.eng.osaka-u.ac.jp (O. Gokcekaya), ozasa@mat.eng.osaka-u.ac.jp (R. Ozasa), tmatsu@md.okayama-u.ac.jp (T. Matsumoto), h.takahashi@teijin-nakashima.co.jp (H. Takahashi), hi.yasui@teijin-nakashima.co.jp (H. Yasui), nakano@mat.eng.osaka-u.ac.jp (T. Nakano).

https://doi.org/10.1016/j.bioadv.2023.213633
Received 17 May 2023; Received in revised form 8 September 2023; Accepted 18 September 2023
Available online 19 September 2023

suggests that earlier and longer osseointegration can inhibit bacterial adhesion and possibly prevent late infection.

In addition to the newly formed bone volume, the bone quality around the implants may also be relevant to postoperative infections. Rheumatoid arthritis (RA) is a risk factor for postoperative infections [26,27]. Our previous studies showed RA to alter the bone microstructure composed of collagen fibers and apatite nanocrystals [28]. The degree of collagen and apatite orientation is an important indicator of bone quality and has been shown to dictate bone mechanical function rather than mineral density [29]. Furthermore, the production of inflammatory cytokines in RA is related to the organization of the bone matrix. Interleukin-6 (IL-6), one of the most abundant cytokines in patients with RA, has been shown to disrupt osteoblast arrangement [30], which is a determinant of bone microstructure anisotropy [31]. We can think of postoperative infections in association with inflammatory cytokine secretion around implants as an influencing cue for bone quality dysfunction.

We aimed to investigate the potential effect of oriented bone matrix organization on bacterial infection. The hypothesis is that living bones inherently possess the antibacterial function triggered by the formation of an organized collagen/apatite microstructure. In the present study, we established a co-culture model of osteoblasts and Gram-negative *Escherichia coli* (*E. coli*) to assess the relationship between the oriented bone matrix and bacterial infection. Osteoblasts were first cultured on titanium alloys to induce osteoblast adhesion and bone matrix production. Subsequently, *E. coli* were cultured on the samples. The number of bacteria that adhered to the titanium alloys and inflammatory responses were evaluated.

2. Materials and methods

2.1. Sample preparation and surface characterization

A gas-atomized Ti-15 mass% Mo-5 mass% Zr-3mass% Al powder was used as the raw material. Two types of samples with a diameter of 15 mm and height of 4.0 mm were fabricated using the laser powder bed fusion (L-PBF) method (M290, EOS, Germany). One has unidirectional groove structures on the surface (Groove). The designed groove pitch and depth were set as 100 μm. The other sample had a flat surface (Flat). The trapped powder particles on the surface were removed by cleaning with fluorine nitric acid, and then ultrasonically washed with acetone, ethanol, and distilled water. All samples were sterilized in an autoclave prior to cell culture.

The surface structure of the fabricated samples was analyzed using three dimensional (3D) laser scanning microscope (OLS5100, Olympus, Tokyo, Japan). Five different areas of each sample were scanned, and three different lines of each image were selected to measure the roughness parameters (*Ra*, *Rsm*, *and Rz*) according to JIS B 0601. Groove pitches and depths were determined as half of *Rsm* and *Rz*, respectively.

2.2. Isolation and culture of osteoblasts

Primary osteoblasts were isolated from the calvariae of neonatal C57BL/6 mice under aseptic conditions. The calvariae were extracted and placed in ice-cold α-modified Eagle's medium (α-MEM; GIBCO, Thermo Fisher Scientific, Waltham, MA). The surrounding fibrous tissue was gently removed. The calvarie were then washed with Hanks' balanced salt solution (HBSS; GIBCO), and treated with collagenase (Fujifilm Wako Pure Chemical, Osaka, Japan)/trypsin (Nacalai Tesque, Kyoto, Japan) five times at 37 °C for 15 min each. The supernatants from the third to fifth treatments were collected in α-MEM. The collections were filtered through a cell strainer (BD Biosciences, San Jose, CA, USA), centrifuged, and the supernatants were removed. The isolated cells were resuspended in α-MEM containing 10 % fetal bovine serum (FBS; GIBCO) and 1 % penicillin and streptomycin (Invitrogen, Carlsbad, CA).

For the short-term culture of cells, isolated cells were seeded onto each sample at a density of 8000 cells/cm^2 and incubated at 37 °C and in 5 % CO_2 for 4 days. For osteogenic induction, cells were seeded at a density of 10,000 cells/cm^2, and after 1 week of cell seeding, the medium was supplemented with 50 μg/mL ascorbic acid (Sigma, St. Louis, MO, USA), 10 mM β-glycerophosphate (Tokyo Kasei, Tokyo, Japan), and 50 nM dexamethasone (MP Bioscience, Solon, OH, USA) at final concentrations. The medium was replaced twice weekly. All animal experiments were approved by the Ethics Committee for Animal Experiments at Osaka University.

2.3. Immunofluorescence staining

After 4 days of culture, cells were fixed with 4 % formaldehyde in phosphate-buffered saline (PBS) for 20 min. After washing with PBST (PBS containing 0.05 % Triton X-100), cells were blocked with PBST containing 1 % normal goat serum (NGS; Invitrogen) for 30 min. Then, the cells were incubated with mouse monoclonal antibodies against vinculin (Sigma-Aldrich) at 4 °C overnight for immunostaining of vinculins. The cells were then washed with PBS and treated with secondary antibodies (Alexa Fluor 546-conjugated anti-mouse IgG; Invitrogen) and Hoechst33342 (Nacalai Tesque) for 2 h at room temperature. For the visualization of F-actin, the cells were treated with Alexa Fluor 488-conjugated phalloidin (Invitrogen). Finally, the cells were washed with PBST and mounted using the ProLong Diamond Antifade Reagent (Invitrogen). The samples were then observed under a fluorescence microscope (BZ-X710; Keyence, Osaka, Japan).

The cells and bone matrices were fixed with 4 % formaldehyde after 21 days of culture to visualize the collagen fibers. Rabbit polyclonal antibodies against collagen type I (Abcam, Cambridge, MA, USA) were used as described above.

2.4. Cell orientation analysis

The degree of cell orientation with respect to the groove direction was quantitatively evaluated based on F-actin-stained images obtained using a fluorescence microscope. Cell orientation was quantitatively analyzed using the Cell Profiler software version 3.1.9 (Broad Institute, Cambridge, MA, USA), and the degree of cell arrangement was calculated using the following equation:

$$r = 2\left\{\left(cos^2\theta\right) - 1/2\right\} \quad (1)$$

where r indicates the degree of cell orientation ($r = 0$ for a random orientation and $r = 1$ for a completely aligned distribution).

2.5. Co-culture system of Escherichia coli and osteoblasts

Gram-negative *E. coli* bacteria (ATCC8739) were purchased from the American Type Culture Collection (Manassas, VA, USA). *E. coli* was incubated using the shake-flask method (37 °C, 120 rpm) in Nutrient Broth (NB) medium. After incubation, the optical densities (OD) at 540 nm of *E. coli* suspensions were measured using a microplate reader (MULTISKAN FC, Thermo Fisher Scientific), and the OD values were adjusted to ~0.5, and then serially diluted in 1/500 NB medium (10^4-fold).

Samples were placed in 24-well plates with α-MEM containing 10 % fetal bovine serum and 1 % penicillin and streptomycin. The isolated osteoblasts were seeded onto the samples at a density of 10000 cells/cm^2. After 7 days of culture, the medium was supplemented with ascorbic acid, β-glycerophosphate, and dexamethasone, as described in this section. The culture medium was changed twice a week. After 4 or 21 days of culture, the supernatants were removed, and 0.9 mL of α-MEM containing 10 % FBS was added to the samples. Additionally, 0.1 mL of the diluted bacteria solutions were added to each sample. The osteoblasts and *E. coli* cells were co-cultured at 37 °C in 5 % CO_2 for 1 day (Fig. 1).

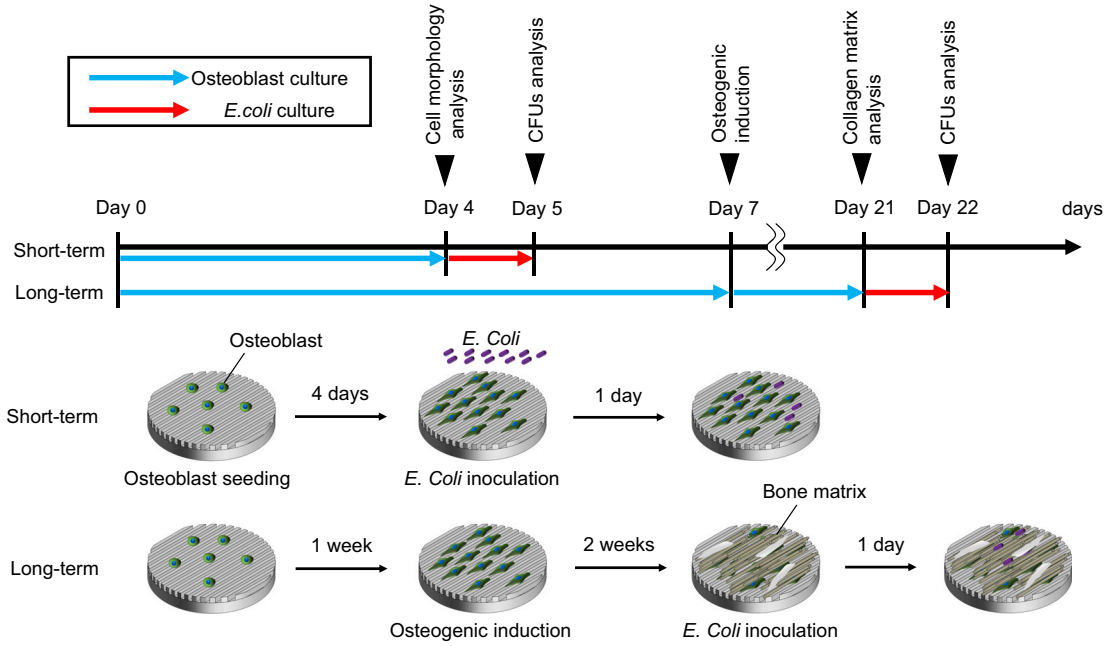

Fig. 1. Schematic illustration of the experimental protocol.

2.6. Cell viability assay

The Viability Detection Kit (DOJINDO, Kumamoto, Japan) was used to quantify cell viability. After the co-culture of *E. coli* and osteoblasts, the cells and bacteria were washed three times with PBS and incubated with CFDA (Carboxyfluorescein diacetate) and PI (Propidium iodine) solutions. The cells and bacteria were observed using a fluorescent microscope (BZ-X710). The green, fluorescent cells were counted as live cells, and red fluorescent cells were excluded as dead cells.

2.7. Quantitative analysis of colony forming unit

Adhered *E. coli* in the samples were collected using a previously reported ultrasonic and mixing method [32,33]. Briefly, the samples were washed twice with PBS and placed in individual test tubes containing 3 mL of PBS. The tubes were capped, sonicated in an ultrasonic bath for 15 min, and mixed by vortexing for 10 s. The collected suspensions were serially diluted 100-fold and spread onto NB agar plates. The agar plates were then incubated at 37 °C overnight. The colony forming units (CFUs) on the agar plates were counted using the Colony Counter 1.0 software (Microtec, Chiba, Japan). When highly aggregated colonies were observed, the samples were removed from this analysis. This software enables counting of single colonies and automatically calculates colony sizes. When overlapping colonies were detected, the number of colonies was estimated using the size of single colonies. The sum of the single colonies and estimated colonies in the overlapping colonies was used in this study.

2.8. Scanning electron microscope (SEM)

The adherent *E. coli* and osteoblasts on the samples were observed using a SEM (S-4800, HITACHI, Tokyo, Japan). After 4 days of cell culture followed by 1 day of co-cultivation, *E. coli* and osteoblasts were rinsed with 0.1 M sodium cacodylate buffer, and fixed with 2 % glutaraldehyde in cacodylate buffer at 4 °C for 30 min. They were then washed with the same buffer and post-fixed with 1 % osmium tetroxide for 1 h. The samples were dehydrated with serial concentration of ethanol (50–100 %), substituted with t-butyl alcohol, and freeze-dried. The samples were sputter-coated (E-1010, HITACHI) with gold for 15 s and observed using SEM at an accelerating voltage of 5 kV.

2.9. Analysis of antimicrobial peptide secretion and protein microarray of inflammatory cytokines and chemokines

The supernatants collected after 1 day of co-culture were centrifuged, and then frozen at −20 °C until the analysis. The release of antimicrobial peptide was evaluated by enzyme-linked immunosorbent assay (ELISA). Mouse β-defensin 2 (DEFB2) and 3 (DEFB3) levels were measured using Mouse Beta-defensin 2 ELISA Kit (MyBioSource, CA, USA) and Mouse Beta-defensin 3 ELISA Kit (MyBioSource), respectively, according to the manufacturer's protocol.

The concentrations of 40 inflammatory cytokines, chemokines, and growth factors in the supernatants ($n = 6$) at 10-fold dilutions were determined using a Quantibody Mouse Inflammation Array I kit (RayBiotech, Inc. Norcross, GA, USA) according to the manufacturer's instructions. This assay enables quantitative analysis of 40 inflammatory markers simultaneously from a single supernatant. Signals (green fluorescence, Cy3 channel, excitation at 555 nm, and emission at 565 nm) were captured using a GenePix 4400 A laser scanner (Molecular Devices, LLC, USA) and extracted using GenePix Pro 7 software (Molecular Devices). Quantitative data analysis was performed using RayBiotech mouse Inflammation Array 1 software (QAM-INF-1_Q-Analyzer). The concentrations of inflammation markers were calculated using standard curves between the concentrations and Cy3 signals. When Cy3 signals were above the upper limit or below the lower limit of the standard curves, the limit values of the curves were used. When the signals of more than half of the samples in both Flat and Groove were below the lower limit of the standard curves, the cytokines were excluded from the analysis.

2.10. Statistical analysis

To compare the data between the two groups, a two-tailed unpaired *t*-test or Mann-Whitney *U* test was used. Statistical significance was set at $P < 0.05$. EZR version 1.41 software was used for the statistical analysis [34].

3. Results

3.1. Surface characterization

3D laser scanning images revealed that the groove surface structures were successfully achieved in Groove samples (Fig. 2(A)). The pitch and depth of grooves were quantitatively analyzed, and Groove had a pitch of 101.6 ± 7.6 μm and a depth of 100.5 ± 9.5 μm. The average surface roughness (*Ra*) of Groove sample was significantly higher than that of Flat (Flat; 5.0 ± 0.3 μm, Groove; 24.5 ± 2.6 μm).

3.2. Osteoblast arrangement

Immunofluorescence images of the cells, cell orientation angle histograms, and degree of cell orientation after 4 days of culture are shown in Fig. 2(B). The osteoblasts on the Groove were preferentially elongated and aligned along the groove direction, whereas cell alignment was not observed on the flat surface. The cell orientation angles in the Groove were distributed about the center of zero, and the degree of cell alignment in the Groove was significantly higher than that in Flat. Type I collagen fibers secreted by the osteoblasts on the Groove tended to orient along the cell alignment direction, while collagen on the Flat

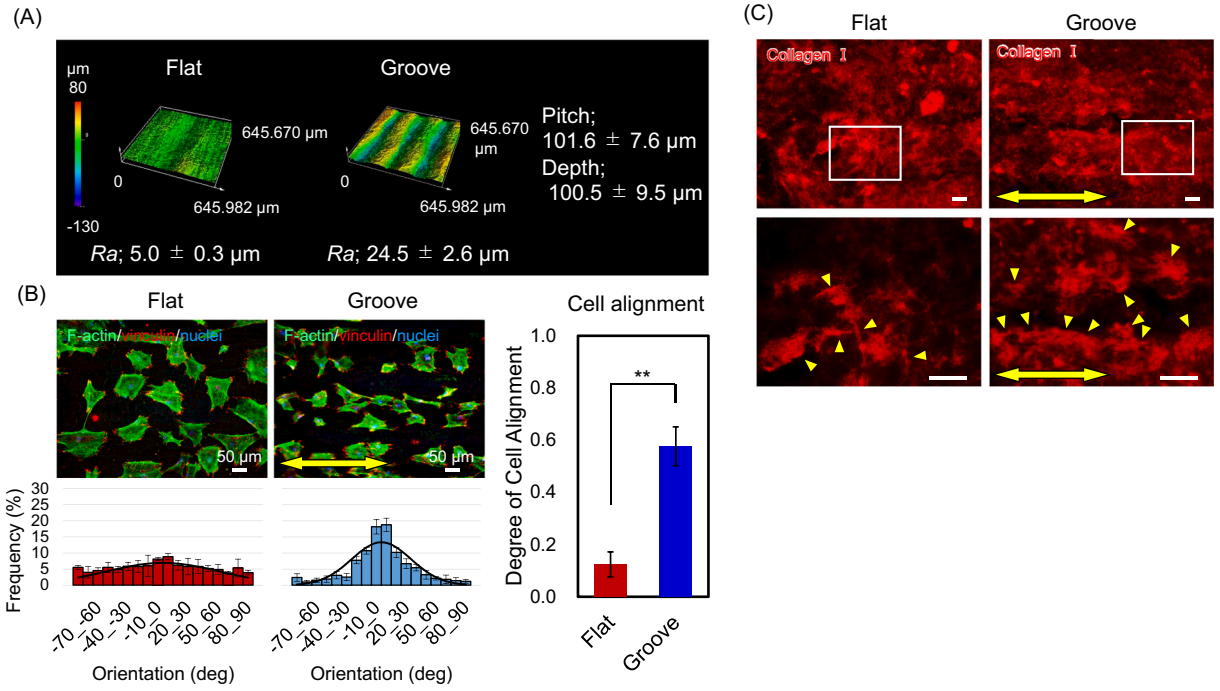

Fig. 2. (A) 3D topographical images of Flat and Groove samples obtained using laser scanning microscope. (B) Immunofluorescence images of osteoblasts, histograms of cell orientation angle, and the degree of cell alignment cultured on Flat and Groove samples. Green: F-actin, blue: nuclei, and red: vinculin. ** $P < 0.01$. (C) Immunofluorescence images of Type I collagen. Arrowheads indicate collagen fiber. On the grooved sample, well-aligned collagen fibers parallel to the groove direction are represented.

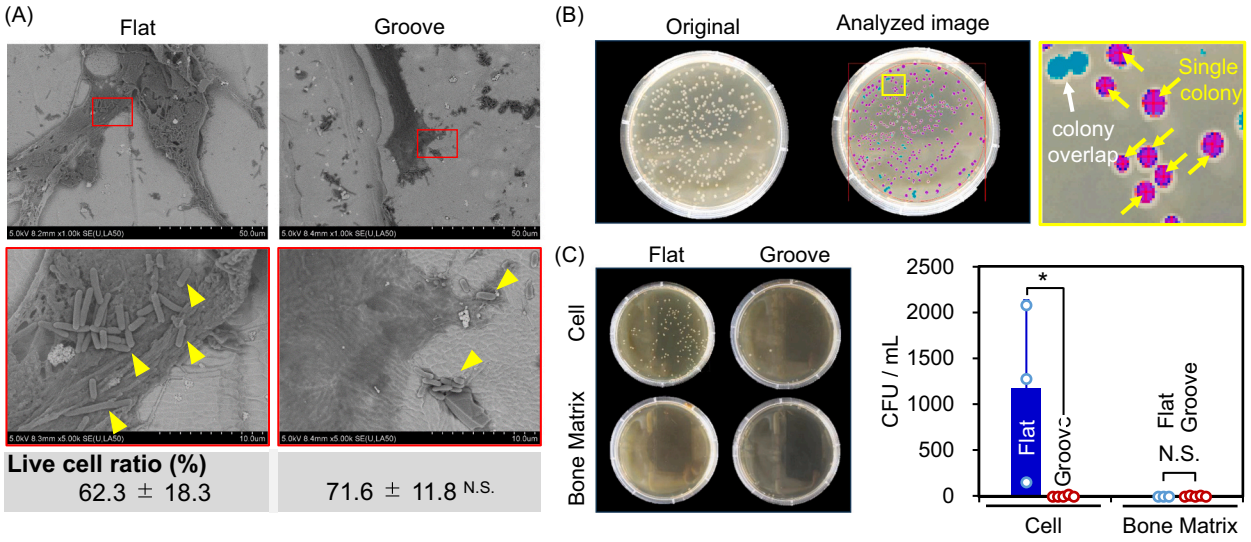

Fig. 3. (A) SEM images of the samples after cultivation of osteoblasts and *E. coli*. Arrowheads indicate *E. coli* adhered to the samples. The live cell ratio of the osteoblasts in coculture with *E. coli*. N.S.; not significant. (B) Representative images of CFU analysis using Colony Counter 1.0 software. (C) Agar plates of each sample and the quantitative result of CFU analysis (100-fold diluted values). * $P < 0.05$ (Mann-Whitney's *U* test).

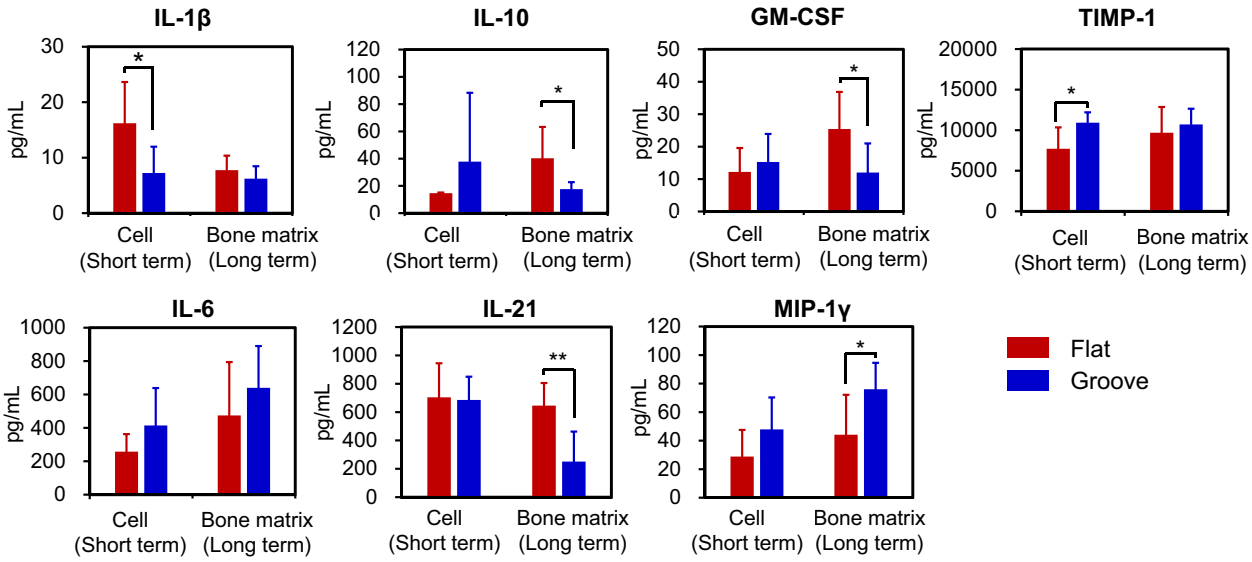

Fig. 4. Quantitative secretion analysis of inflammation markers in the supernatants after osteoblast-*E. coli* co-culture. The 10-fold diluted values were used in this Figure. * $P < 0.05$, ** $P < 0.01$.

surface was not oriented (Fig. 2(C)).

3.3. Effects of the osteoblast arrangement and secreted matrix orientation on E. coli adhesion

The SEM images of the samples with cells after co-cultivation are shown in Fig. 3(A). In the Flat sample, many *E. coli* adhered to osteoblasts, whereas the number of adhered bacteria decreased in the Groove sample.

The number of adhered *E. coli* on the samples was quantitatively analyzed using the agar plate method. Highly aggregated colonies were observed on two plates of Flat with cells. These were excluded from this study. Representative CFUs counted images, images of the agar plates cultured overnight, and the CFU per mL of each sample are shown in Fig. 3(B, C). The CFU of Groove with cells was significantly lower than that of Flat. Flat and Groove with the bone matrix exhibited almost no CFUs, and no significant differences were observed between the Flat and Groove with the bone matrix.

3.4. Cell viability after co-culture of E. coli and osteoblasts

Cell viability after co-culture of *E. coli* and osteoblasts was assessed by live/dead staining. The quantitative analysis of fluorescent microscope images of the samples showed that the cell viability was not significantly affected by the unidirectional groove structure.

3.5. Secretions of inflammatory cytokines and antimicrobial peptides

Among the 40 inflammatory markers, 6 were significantly different between the Flat- and Groove-type samples. The levels of IL-1β (Interleukin-1β) in Groove with cells were significantly lower than that in Flat (Fig. 4). Groove with cells showed significantly greater levels of TIMP-1 (Tissue inhibitor of metalloproteinase-1) than Flat. IL-10 (Interleukin-10), IL-21 (Interleukin-21), and GM-CSF (Granulocyte-macrophage colony-stimulating factor) in the Groove with bone matrix were significantly decreased compared to those in the Flat. Groove with bone matrix showed significantly higher expression of MIP-1γ (Macrophage inflammatory protein-1 gamma) than Flat. In contrast, no significant differences were observed between Flat and Groove for IL-6 (Interleukin-6). The secretion levels of DEFB2 (coding β-defensin2) and DEFB3 (coding β-defensin3) after 1 day of co-culture are shown in Fig. 5. Groove with bone matrix showed significantly higher levels of DEFB2 and DEFB3 than Flat.

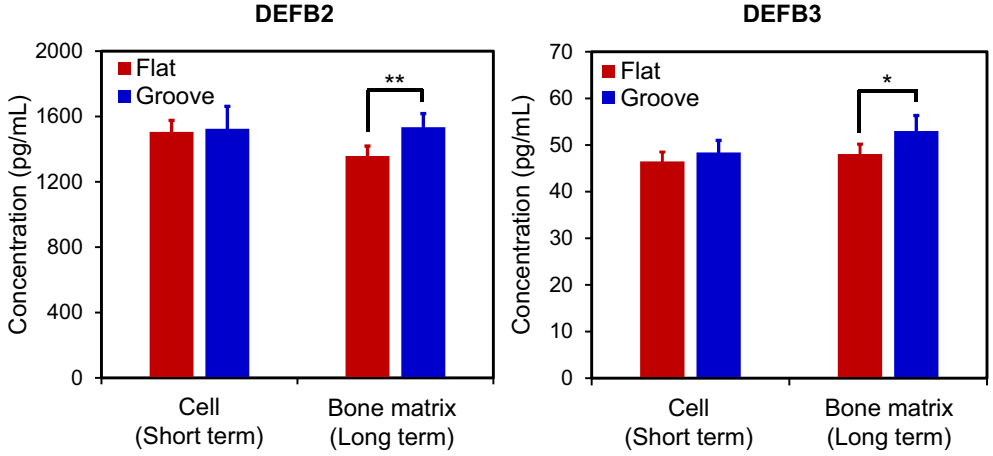

Fig. 5. Quantitative results of DEFB2 and DEFB3 secretions using ELISA analysis. * $P < 0.05$, ** $P < 0.01$.

4. Discussion

Bone functionalization has been investigated by focusing on only bone mineral density as an indicator for decades. The microorganization of the bone matrix has been increasingly recognized as a bone quality index and its importance in bone mechanical functions has been now widely accepted all over the world. The degree of preferential collagen and apatite orientation has been discovered as an indicator of trabecular bone health [35]. In addition, deteriorated collagen and apatite microstructures are the primary factor of bone dysfunction involving cancer [36], osteoporosis [37], and RA [28]. Therefore, maintaining bone microstructure could be essential for preserving bone tissues in healthy conditions. A clinical study also reported that an open bone fracture is a risk factor for osteomyelitis, a bone infection caused by bacteria [38]. Indeed, during the bone regeneration process, the recovery of the collagen and apatite orientation requires a longer period than that of the bone mineral density [29]. These suggest the possible association between disorganized collagen and apatite microstructure and the risk of bacterial infection. However, the relationship between bone matrix organization and bacterial infection has not yet been reported. This is the first study to investigate the effects of the bone-mimetic organized microstructure of bone matrix on bacterial infection.

Our previous studies have demonstrated that anisotropic topography with optimal dimensions induces osteoblast elongation and alignment [39–41]. The aligned osteoblasts produce preferentially oriented collagen matrix parallel to the direction of the cell body [31]. In addition, L-PBF-fabricated unidirectional microgrooves have been reported to control the osteoblast alignment and further the bone matrix organization [42]. In this study, we prepared a unidirectional groove structure on medically licensed Ti-15Mo-5Zr-3Al alloy using L-PBF method. Micrometer-scaled groove structure was successfully fabricated by L-PBF. Immunofluorescence analysis revealed preferential alignment of osteoblasts along the groove direction. The collagen matrix produced by the aligned osteoblasts was oriented parallel to the direction of the osteoblast alignment, which is consistent with our previous study [31].

To demonstrate the effectiveness of the antimicrobial activities of implants, co-culture models of osteoblasts and bacteria, such as *Staphylococcus aureus*, *Staphylococcus epidermidis*, and *E. coli* have been established in previous reports [32,33,43,44]. In these models, osteoblasts and bacteria were simultaneously seeded, or bacteria were inoculated (several hours) after seeding of osteoblasts on the implants, as the antimicrobial properties were provided for the implant surfaces to inhibit bacterial adhesion. We prepared samples with osteoblast attachment and bone matrix secretion and then *E. coli* was co-cultured to evaluate the effects of preferentially oriented osteoblasts and bone formation by groove structures on bacterial adhesion.

Quantitative analysis demonstrated that the amount of adhered *E. coli* on Groove with cells was significantly lower than that on the Flat. SEM images showed an apparently increased number of *E. coli* cells adhering to randomly oriented osteoblasts compared to that on highly oriented osteoblasts, indicating that the aligned osteoblasts could impede *E. coli* adhesion. Bacteria could not only attach to implant surfaces but also to host cells. The adhesion of *E. coli* to host cells requires a multistep process [45]. Bacteria initially attach to cells without undergoing molecular interactions. In this step, the glycocalyx, a layer of glycosylated proteins and lipids covers host cells and inhibits the binding of bacterial adhesion to ligands on the cell surface. Bacteria easily detach from the glycocalyx layer on their cell surface. Subsequently, bacterial adhesions bind to their target receptors, resulting in bacterial infection. Thus, the conditions of the glycocalyx layer on the cells are possibly related to the inhibitory effect on *E. coli* adherence to highly oriented osteoblasts. A previous study revealed that osteoblasts were coated with a glycocalyx-rich layer [46], and the distribution of this layer was altered in accordance with the cytoskeletal reorganization induced by shear stress. The elongated cells under shear stress stimulation are covered by the uniformly redistributed glycocalyx layer [47–49]. These reports indicate the interesting findings of relations between the host cell cytoskeletons and bacterial adhesion. The uniformly covered glycocalyx layer on the aligned osteoblasts may impede *E. coli* adherence. Our next study will investigate the effects of glycocalyx layer uniformity of aligned osteoblasts on bacterial attachment. In spite, both Flat and Groove samples with bone matrix showed low CFU, and no significant differences were observed. This suggests that osteoblast-produced bone matrix shields from *E. coli* adhering to cells.

Bacterial attachment activates the immune system to prevent bacterial colonization [50]. Although osteoblasts have been primarily studied as bone-forming cells, recent studies have revealed that they can also be characterized as inflammatory cells. The release of inflammatory cytokines by osteoblasts in response to bacterial stimulation has been described [51,52]. In this study, the secretion of inflammatory cytokines was evaluated quantitatively. The cells on Flat exhibited the significantly increased secretion of IL-1β, which was found to be a biomarker for the detection of inflammatory diseases such as periprosthetic joint infection [53,54], compared with Groove. This was consistent with our CFU results. Interestingly, the secretion levels of inflammatory cytokines were clearly affected by anisotropic bone matrix secretion, whereas no significant differences were observed in the CFU analysis. Organized texture-controlled bone matrix showed significantly lower secretion of IL-10, GM-CSF, and IL-21 than Flat. Inflammatory cytokines have been reported to be indicators of bacterial infections. The secretion levels of IL-10 [54,55], GM-CSF [56,57], and IL-21 [58,59] in the synovial fluid and plasma of RA, PJI, and periodontitis patients have been investigated, and these levels in patients with inflammatory diseases have been reported to be upregulated compared to those in healthy or aseptic patients. Thus, the decreased IL-10, GM-CSF, and IL-21 levels in the Groove with bone matrix indicated that the formation of preferentially oriented bone could lead to lower *E. coli* adhesion than that of non-oriented bone. This might result in decreased severity of bacterial infections. In contrast, the significant increase of MIP-1γ in Groove with bone matrix compared with Flat was shown. MIP-1γ has been reported to enhance the differentiation, activation, and survival of osteoclasts during bone resorption [60,61]. This suggests that infected bone tissues may be immediately resorbed by osteoclasts that are activated through MIP-1γ secretion.

The inflammatory responses are strictly controlled under the molecular interactions involving the secretion of antimicrobial peptides. The antimicrobial peptides β-defensins are expressed in mammalian cells in response to bacterial infections [62,63], and have been shown to have neutralizing effects on the proinflammatory response [64]. For instance, the release of TNF-alpha and IL-6 in LPS-treated mice was significantly suppressed in the presence of human β-defensin 3, and pro-inflammatory protein and gene expression were inhibited [65]. In the present study, the secretion levels of β-defensin 2 and β-defensin 3 of aligned osteoblasts with bone matrix were significantly higher than those in the Flat. This indicates that the anisotropic bone matrix suppresses inflammatory cytokines through the production of β-defensin 2 and β-defensin 3. Additionally, β-defensins have been found to have broad antimicrobial activities [64]. The inhibitory effects of human β-defensin 2 on biofilm formation by Gram-negative bacteria have been previously demonstrated [66,67]. Human β-defensin 3 has antimicrobial activity against Gram-negative and -positive bacteria [68,69]. These results indicate that higher secretion of β-defensin 2 and β-defensin 3 could provide greater resistance to bacterial adhesion and biofilm formation. Overall, the formation of an oriented collagen/apatite matrix induced by a unidirectional groove structure could possess the excellent potential for host defense against *E. coli* infection due to its higher expression of antimicrobial peptides. The hypothesized mechanism is illustrated in Fig. 6.

The novel findings of our study are as follows: First, the alignment of osteoblasts on a unidirectional groove structure has inhibited *E. coli* adhesion to them. Bone matrix production also prevented the adhesion of *E. coli* to material surfaces. This is evidenced by SEM and CFU analysis

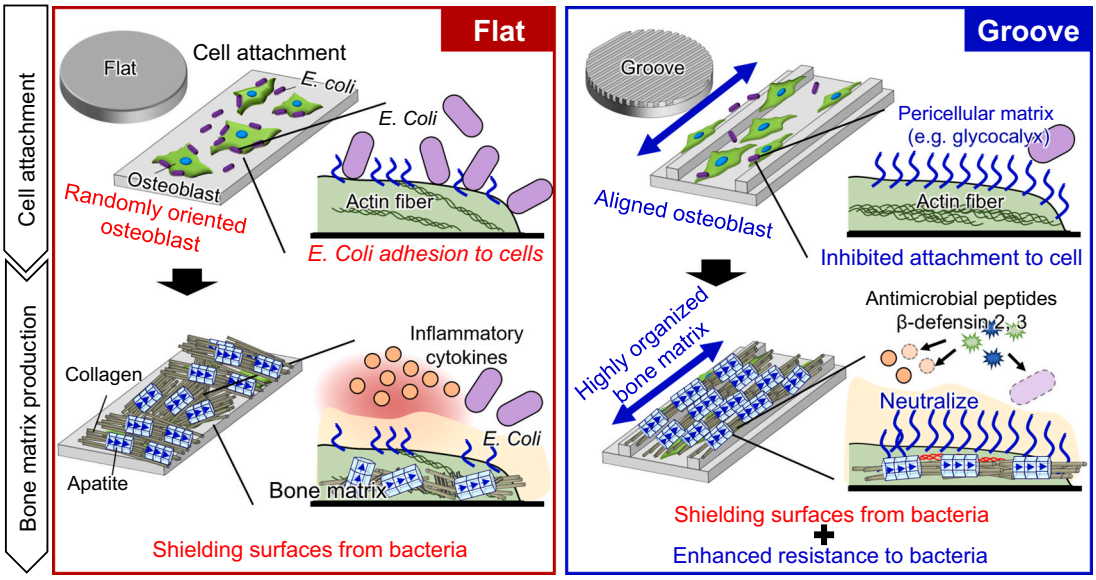

Fig. 6. A hypothesized mechanism of resistance of highly organized bone to *E. coli* infection.

after co-culture of *E. coli* and osteoblast. Second, the highly oriented collagen/apatite matrix could possess great host defense potential against *E. coli* infection through the higher secretion of the antimicrobial peptides, β-defensin 2 and β-defensin 3. These peptides might neutralize the proinflammatory cytokine production. To the best of our knowledge, this is the first study to demonstrate the antimicrobial activity of the highly organized collagen/apatite matrix controlled by a material surface characteristic.

Our recent research developed a new intervertebral spacer with an original honeycomb tree structure (HTS) design that has a unidirectional microgroove structure [42,70]. This spacer exhibited greater interfacial strength and earlier induction of bone with a preferentially oriented collagen/apatite microstructure than the conventional gold standard autologous bone graft. Additionally, HTS guided the alignment of osteocytes along groove direction, indicating that the osteocytes sense principal loading stress along the cephalocaudal axis [71,72]. Thus, HTS spacer enables the maintenance of long-term bone health. The results of our present study suggest that intervertebral spacers with HTS have a great advantage of high resistance to *E. coli* infection through the induction of preferentially oriented bone.

This study has some limitations. First, the secretion levels of inflammatory markers were overestimated to some extent as values lower than the minimum of the calibration curves were replaced by the lower limit. Second, Gram-negative *E. coli* was used in this study, although many clinical studies have revealed that the main causative bacteria in postoperative infections are Gram-positive methicillin-resistant *Staphylococcus aureus* (*S. aureus*) [73,74]. However, infections caused by Gram-negative bacteria have a higher risk of aseptic loosening after revision surgery due to higher lipopolysaccharide (LPS)-induced osteoclast differentiation than those caused by Gram-positive bacteria [75]. Thus, antimicrobial activity against Gram-negative and -positive bacteria is crucial.

5. Conclusion

A co-culture model of osteoblasts and *E. coli* was developed to investigate the effects of preferentially oriented bone formation on bacterial infections. The groove structure successfully induced the alignment of osteoblasts and bone matrix along the groove direction. The adhesion of *E. coli* to host cells was significantly reduced in the aligned osteoblasts. The production of bone matrix by osteoblasts also decreased *E. coli* adhesion. Additionally, the secretion of inflammatory markers in response to *E. coli* stimulation was altered depending on the anisotropy of osteoblasts and their produced bone matrix organization. The organized bone matrix led to decreased inflammatory cytokine secretion in response to *E. coli* stimulation. The results indicate a great potential for the oriented organization of bone matrix on infection resistance. Notably, significantly increased secretion of antimicrobial peptides was observed in the oriented bone matrix compared to that in the non-oriented bone matrix. Our findings provide novel infection mechanisms and an anti-infection strategy for implant development.

Author statement

The manuscript or a very similar manuscript has not been published, nor is under consideration by any other journal.

CRediT authorship contribution statement

Ryota Watanabe: Formal analysis, Investigation, Methodology, Visualization, Writing – original draft. **Aira Matsugaki:** Conceptualization, Investigation, Data curation, Methodology, Validation, Writing – review & editing. **Ozkan Gokcekaya:** Investigation, Data curation. **Ryosuke Ozasa:** Investigation, Data curation. **Takuya Matsumoto:** Validation, Supervision. **Hiroyuki Takahashi:** Validation, Supervision. **Hidekazu Yasui:** Validation, Supervision. **Takayoshi Nakano:** Conceptualization, Methodology, Validation, Writing – review & editing, Supervision, Project administration, Funding acquisition.

Declaration of competing interest

Ryota Watanabe, Hiroyuki Takahashi, and Hidekazu Yasui are employees of Teijin Nakashima Medical, a manufacturer of orthopedic implants. The other authors declare that they have no conflicts of interest.

Data availability

Data will be made available on request.

Acknowledgments

This study was supported by JST-CREST (grant numbers JPMJCR22L5, JPMJCR2194), and Grant-in-Aid for Scientific Research

(A) (grant number 23H00235) from the Japan Society for the Promotion of Science (JSPS).

References

[1] C. Cathleen, C. Bernard, Knee arthroplasty surgical site infection rates over a ten-year period at a community hospital, Am. J. Infect. Control 41 (2013) S112–S113, https://doi.org/10.1016/j.ajic.2013.03.228.

[2] S.P. Nota, Y. Braun, D. Ring, J.H. Schwab, Incidence of surgical site infection after spine surgery: what is the impact of the definition of infection? Clin. Orthop. Relat. Res. 473 (2015) 1612–1619, https://doi.org/10.1007/s11999-014-3933-y.

[3] B. Zmistowski, J.A. Karam, J.B. Durinka, D.S. Casper, J. Parvizi, Periprosthetic joint infection increases the risk of one-year mortality, J. Bone Joint Surg. Am. 95 (2013) 2177–2184, https://doi.org/10.2106/JBJS.L.00789.

[4] S.M. Kurtz, E. Lau, H. Watson, J.K. Schmier, J. Parvizi, Economic burden of periprosthetic joint infection in the United States, J. Arthroplast. 27 (Supplement) (2012), https://doi.org/10.1016/j.arth.2012.02.022 (61–5.e1).

[5] D.S. Casper, B. Zmistowski, D.A. Hollern, A.S. Hilibrand, A.R. Vaccaro, G. D. Schroeder, C.K. Kepler, The effect of postoperative spinal infections on patient mortality, Spine 43 (2018) 223–227, https://doi.org/10.1097/BRS.0000000000002277.

[6] A.M. Schwartz, K.X. Farley, G.N. Guild, T.L. Bradbury Jr., Projections and epidemiology of revision hip and knee arthroplasty in the United States to 2030, J. Arthroplasty 35 (2020) S79–S85, https://doi.org/10.1016/j.arth.2020.02.030.

[7] S.S. Rajaee, H.W. Bae, L.E. Kanim, R.B. Delamarter, Spinal fusion in the United States: analysis of trends from 1998 to 2008, Spine 37 (2012) 67–76, https://doi.org/10.1097/BRS.0b013e31820cccfb.

[8] J.S. Smith, C.I. Shaffrey, C.A. Sansur, S.H. Berven, K.M. Fu, P.A. Broadstone, T. J. Choma, M.J. Goytan, H.H. Noordeen, D.R. Knapp Jr., R.A. Hart, W. F. Donaldson 3rd, D.W. Polly Jr., J.H. Perra, O. Boachie-Adjei, Scoliosis Research Society Morbidity and Mortality Committee, Rates of infection after spine surgery based on 108,419 procedures: a report from the Scoliosis Research Society Morbidity and Mortality Committee, Spine 36 (2011) 556–563, https://doi.org/10.1097/BRS.0b013e3181eadd41.

[9] J. Chahoud, Z. Kanafani, S.S. Kanj, Surgical site infections following spine surgery: eliminating the controversies in the diagnosis, Front. Med. (Lausanne) 1 (2014) 7, https://doi.org/10.3389/fmed.2014.00007.

[10] H. Segawa, D.T. Tsukayama, R.F. Kyle, D.A. Becker, R.B. Gustilo, Infection after total knee arthroplasty. A retrospective study of the treatment of eighty-one infections, J. Bone Joint Surg. Am. 81 (1999) 1434–1445, https://doi.org/10.2106/00004623-199910000-00008.

[11] K. Huotari, M. Peltola, E. Jämsen, The incidence of late prosthetic joint infections: a registry-based study of 112,708 primary hip and knee replacements, Acta Orthop. 86 (2015) 321–325, https://doi.org/10.3109/17453674.2015.1035173.

[12] K. Maruo, S.H. Berven, Outcome and treatment of postoperative spine surgical site infections: predictors of treatment success and failure, J. Orthop. Sci. 19 (2014) 398–404, https://doi.org/10.1007/s00776-014-0545-z.

[13] B.R. Richards, K.M. Emara, Delayed infections after posterior TSRH spinal instrumentation for idiopathic scoliosis: revisited, Spine 26 (2001) 1990–1996, https://doi.org/10.1097/00007632-200109150-00009.

[14] T.J. Kowalski, E.F. Berbari, P.M. Huddleston, J.M. Steckelberg, J.N. Mandrekar, D. R. Osmon, The management and outcome of spinal implant infections: contemporary retrospective cohort study, Clin. Infect. Dis. 44 (2007) 913–920, https://doi.org/10.1086/512194.

[15] T. Morimoto, H. Hirata, S. Eto, A. Hashimoto, S. Kii, T. Kobayashi, M. Tsukamoto, T. Yoshihara, Y. Toda, M. Mawatari, Development of silver-containing hydroxyapatite-coated antimicrobial implants for orthopaedic and spinal surgery, Medicina (Kaunas) 58 (2022) 519, https://doi.org/10.3390/medicina58040519.

[16] O.D. Savvidou, A. Kaspiris, I. Trikoupis, G. Kakouratos, S. Goumenos, D. Melissaridou, P.J. Papagelopoulos, Efficacy of antimicrobial coated orthopaedic implants on the prevention of periprosthetic infections: a systematic review and meta-analysis, J. Bone Jt. Infect. 5 (2020) 212–222, https://doi.org/10.7150/jbji.44839.

[17] M. Fiore, A. Sambri, R. Zucchini, C. Giannini, D.M. Donati, M. De Paolis, Silver-coated megaprosthesis in prevention and treatment of peri-prosthetic infections: a systematic review and meta-analysis about efficacy and toxicity in primary and revision surgery, Eur. J. Orthop. Surg. Traumatol. 31 (2021) 201–220, https://doi.org/10.1007/s00590-020-02779-z.

[18] I. Noda, F. Miyaji, Y. Ando, H. Miyamoto, T. Shimazaki, Y. Yonekura, M. Miyazaki, M. Mawatari, T. Hotokebuchi, Development of novel thermal sprayed antibacterial coating and evaluation of release properties of silver ions, J. Biomed. Mater. Res. B Appl. Biomater. 89 (2009) 456–465, https://doi.org/10.1002/jbm.b.31235.

[19] B. Wang, A. Bian, F. Jia, J. Lan, H. Yang, K. Yan, L. Xie, H. Qiao, X. Chang, H. Lin, H. Zhang, Y. Huang, "Dual-functional" strontium titanate nanotubes designed based on fusion peptides simultaneously enhancing anti-infection and osseointegration, Biomater. Adv. 133 (2022), 112650, https://doi.org/10.1016/j.msec.2022.112650.

[20] B. Wang, Z. Wu, S. Wang, S. Wang, Q. Niu, Y. Wu, F. Jia, A. Bian, L. Xie, H. Qiao, X. Chang, H. Lin, H. Zhang, Y. Huang, Mg/cu-doped TiO_2 nanotube array: a novel dual-function system with self-antibacterial activity and excellent cell compatibility, Mater. Sci. Eng. C 128 (2021), 112322, https://doi.org/10.1016/j.msec.2021.112322.

[21] B. Wang, Z. Wu, J. Lan, Y. Li, L. Xie, X. Huang, A. Zhang, H. Qiao, X. Chang, H. Lin, H. Zhang, T. Li, Y. Huang, Surface modification of titanium implants by silk fibroin/Ag co-functionalized strontium titanate nanotubes for inhibition of bacterial-associated infection and enhancement of in vivo osseointegration, Surf. Coat. Technol. 405 (2021), 126700, https://doi.org/10.1016/j.surfcoat.2020.126700.

[22] Y. Huang, Y. Zhang, M. Li, H. Yang, J. Liang, Y. Chen, Y. Zhang, X. Huang, L. Xie, H. Lin, H. Qiao, J. Lan, Physicochemical, osteogenic and antimicrobial properties of graphene oxide reinforced silver/strontium-doped hydroxyapatite on titanium for potential orthopedic applications, Surf. Coat. Technol. 446 (2022), 128788, https://doi.org/10.1016/j.surfcoat.2022.128788.

[23] B. Wang, Y. Li, S. Wang, F. Jia, A. Bian, K. Wang, L. Xie, K. Yan, H. Qiao, H. Lin, J. Lan, Y. Huang, Electrodeposited dopamine/strontium-doped hydroxyapatite composite coating on pure zinc for anti-corrosion, antimicrobial and osteogenesis, Mater. Sci. Eng. C 129 (2021), 112387, https://doi.org/10.1016/j.msec.2021.112387.

[24] A.G. Gristina, Biomaterial-centered infection: microbial adhesion versus tissue integration, Science 237 (1987) 1588–1595, https://doi.org/10.1126/science.3629258.

[25] H.J. Busscher, H.C. van der Mei, G. Subbiahdoss, P.C. Jutte, J.J. van den Dungen, S. A. Zaat, M.J. Schultz, D.W. Grainger, Biomaterial-associated infection: locating the finish line in the race for the surface, Sci. Transl. Med. 4 (2012), 153rv10, https://doi.org/10.1126/scitranslmed.3004528.

[26] S. Zhang, L. Wang, L. Bao, H. Sun, F. Feng, J. Shan, H. Tang, Does rheumatoid arthritis affect the infection and complications rates of spinal surgery? A systematic review and meta-analysis, World Neurosurg. 145 (2021) 260–266, https://doi.org/10.1016/j.wneu.2020.09.039.

[27] B. Ravi, B. Escott, P.S. Shah, R. Jenkinson, J. Chahal, E. Bogoch, H. Kreder, G. Hawker, A systematic review and meta-analysis comparing complications following total joint arthroplasty for rheumatoid arthritis versus for osteoarthritis, Arthritis Rheum. 64 (2012) 3839–3849, https://doi.org/10.1002/art.37690.

[28] R. Ozasa, A. Matsugaki, T. Ishimoto, S. Kamura, H. Yoshida, M. Magi, Y. Matsumoto, K. Sakuraba, K. Fujimura, H. Miyahara, T. Nakano, Bone fragility via degradation of bone quality featured by collagen/apatite micro-arrangement in human rheumatic arthritis, Bone 155 (2022), 116261, https://doi.org/10.1016/j.bone.2021.116261.

[29] T. Ishimoto, T. Nakano, Y. Umakoshi, M. Yamamoto, Y. Tabata, Degree of biological apatite c-axis orientation rather than bone mineral density controls mechanical function in bone regenerated using recombinant bone morphogenetic protein-2, J. Bone Miner. Res. 28 (2013) 1170–1179, https://doi.org/10.1002/jbmr.1825.

[30] A. Matsugaki, S. Matsumoto, T. Nakano, A novel role of interleukin-6 as a regulatory factor of inflammation-associated deterioration in osteoblast arrangement, Int. J. Mol. Sci. 21 (2020) 1–11, https://doi.org/10.3390/ijms21186659.

[31] A. Matsugaki, Y. Isobe, T. Saku, T. Nakano, Quantitative regulation of bone-mimetic, oriented collagen/apatite matrix structure depends on the degree of osteoblast alignment on oriented collagen substrates, J. Biomed. Mater. Res. A 103 (2015) 489–499, https://doi.org/10.1002/jbm.a.35189.

[32] S. Zaatreh, K. Wegner, M. Strauß, J. Pasold, W. Mittelmeier, A. Podbielski, B. Kreikemeyer, R. Bader, Co-culture of *S. epidermidis* and human osteoblasts on implant surfaces: an advanced in vitro model for implant-associated infections, PLOS ONE 11 (2016), e0151534, https://doi.org/10.1371/journal.pone.0151534.

[33] Y. Yang, H. Ao, Y. Wang, W. Lin, S. Yang, S. Zhang, Z. Yu, T. Tang, Cytocompatibility with osteogenic cells and enhanced in vivo anti-infection potential of quaternized chitosan-loaded titania nanotubes, Bone Res. 4 (2016) 16027, https://doi.org/10.1038/boneres.2016.27.

[34] Y. Kanda, Investigation of the freely available easy-to-use software "EZR" for medical statistics, Bone Marrow Transplant. 48 (2013) 452–458, https://doi.org/10.1038/bmt.2012.244.

[35] T. Ishimoto, K. Yamada, H. Takahashi, M. Takahata, M. Ito, T. Hanawa, T. Nakano, Trabecular health of vertebrae based on anisotropy in trabecular architecture and collagen/apatite micro-arrangement after implantation of intervertebral fusion cages in the sheep spine, Bone. 108 (2018) 25–33, https://doi.org/10.1016/j.bone.2017.12.012.

[36] A. Sekita, A. Matsugaki, T. Nakano, Disruption of collagen/apatite alignment impairs bone mechanical function in osteoblastic metastasis induced by prostate cancer, Bone 97 (2017) 83–93, https://doi.org/10.1016/j.bone.2017.01.004.

[37] R. Ozasa, T. Ishimoto, S. Miyabe, J. Hashimoto, M. Hirao, H. Yoshikawa, T. Nakano, Osteoporosis changes collagen/apatite orientation and Young's modulus in vertebral cortical bone of rat, Calcif. Tissue Int. 104 (2019) 449–460, https://doi.org/10.1007/s00223-018-0508-z.

[38] G. Slyamova, A. Gusmanov, A. Batpenov, N. Kaliev, D. Viderman, Risk factors for postoperative osteomyelitis among patients after bone fracture: a matched case-control study, J. Clin. Med. 11 (2022) 6072, https://doi.org/10.3390/jcm11206072.

[39] D. Franco, M. Klingauf, M. Bednarzik, M. Cecchini, V. Kurtcuoglu, J. Gobrecht, D. Poulikakos, A. Ferrari, Control of initial endothelial spreading by topographic activation of focal adhesion kinase, Soft Matter 7 (2011) 7313–7324, https://doi.org/10.1039/c1sm05191a.

[40] M. Schernthaner, G. Leitinger, H. Wolinski, S.D. Kohlwein, B. Reisinger, R.A. Barb, W.F. Graier, J. Heitz, K. Groschner, Enhanced Ca2+ entry and tyrosine phosphorylation mediate nanostructure-induced endothelial proliferation, J. Nanomater. 2013 (2013), 251063, https://doi.org/10.1155/2013/251063.

[41] S. Lee, A. Matsugaki, T. Kasuga, T. Nakano, Development of bifunctional oriented bioactive glass/poly(lactic acid) composite scaffolds to control osteoblast alignment and proliferation, J. Biomed. Mater. Res. A 107 (2019) 1031–1041, https://doi.org/10.1002/jbm.a.36619.

[42] T. Ishimoto, Y. Kobayashi, M. Takahata, M. Ito, A. Matsugaki, H. Takahashi, R. Watanabe, T. Inoue, T. Matsuzaka, R. Ozasa, T. Hanawa, K. Yokota, Y. Nakashima, T. Nakano, Outstanding in vivo mechanical integrity of additively manufactured spinal cages with a novel "honeycomb tree structure" design via guiding bone matrix orientation, Spine J. 22 (2022) 1742–1757, https://doi.org/10.1016/j.spinee.2022.05.006.
[43] L. Chu, Y. Yang, S. Yang, Q. Fan, Z. Yu, X.L. Hu, T.D. James, X.P. He, T. Tang, Preferential colonization of osteoblasts over co-cultured bacteria on a bifunctional biomaterial surface, Front. Microbiol. 9 (2018) 2219, https://doi.org/10.3389/fmicb.2018.02219.
[44] L. Crémet, A. Broquet, B. Brulin, C. Jacqueline, S. Dauvergne, R. Brion, K. Asehnoune, S. Corvec, D. Heymann, N. Caroff, Pathogenic potential of *Escherichia coli* clinical strains from orthopedic implant infections towards human osteoblastic cells, Pathog. Dis. 73 (2015), ftv065, https://doi.org/10.1093/femspd/ftv065.
[45] X. Pierrat, J.P.H. Wong, Z. Al-Mayyah, A. Persat, The Mammalian membrane microenvironment regulates the sequential attachment of bacteria to host cells, mBio 12 (2021), e0139221, https://doi.org/10.1128/mBio.01392-21.
[46] G.C. Reilly, T.R. Haut, C.E. Yellowley, H.J. Donahue, C.R. Jacobs, Fluid flow induced PGE2 release by bone cells is reduced by glycocalyx degradation whereas calcium signals are not, Biorheology 40 (2003) 591–603.
[47] Y. Yao, A. Rabodzey, C.F. Dewey Jr., Glycocalyx modulates the motility and proliferative response of vascular endothelium to fluid shear stress, Am. J. Physiol. Heart Circ. Physiol. 293 (2007) H1023–H1030, https://doi.org/10.1152/ajpheart.00162.2007.
[48] Y. Zeng, J.M. Tarbell, The adaptive remodeling of endothelial glycocalyx in response to fluid shear stress, PloS One 9 (2014), e86249, https://doi.org/10.1371/journal.pone.0086249.
[49] W. Li, W. Wang, Structural alteration of the endothelial glycocalyx: contribution of the actin cytoskeleton, Biomech. Model. Mechanobiol. 17 (2018) 147–158, https://doi.org/10.1007/s10237-017-0950-2.
[50] G. Subbiahdoss, R. Kuijer, D.W. Grijpma, H.C. van der Mei, H.J. Busscher, Microbial biofilm growth vs. tissue integration: "the race for the surface" experimentally studied, Acta Biomater. 5 (2009) 1399–1404, https://doi.org/10.1016/j.actbio.2008.12.011.
[51] U. Dapunt, T. Giese, S. Stegmaier, A. Moghaddam, G.M. Hänsch, The osteoblast as an inflammatory cell: production of cytokines in response to bacteria and components of bacterial biofilms, BMC Musculoskelet. Disord. 17 (2016) 243, https://doi.org/10.1186/s12891-016-1091-y.
[52] I. Marriott, D.L. Gray, S.L. Tranguch, V.G. Fowler Jr., M. Stryjewski, L. Scott Levin, M.C. Hudson, K.L. Bost, Osteoblasts express the inflammatory cytokine interleukin-6 in a murine model of *Staphylococcus aureus* osteomyelitis and infected human bone tissue, Am. J. Pathol. 164 (2004) 1399–1406, https://doi.org/10.1016/S0002-9440(10)63226-9.
[53] H. Wang, L. Qin, J. Wang, W. Huang, Synovial fluid IL-1β appears useful for the diagnosis of chronic periprosthetic joint infection, J. Orthop. Surg. Res. 16 (2021) 144, https://doi.org/10.1186/s13018-021-02296-7.
[54] L. Qin, C. Du, J. Yang, H. Wang, X. Su, L. Wei, C. Zhao, C. Chen, H. Chen, N. Hu, W. Huang, Synovial fluid interleukin levels cannot distinguish between prosthetic joint infection and active rheumatoid arthritis after hip or knee arthroplasty, Diagnostics (Basel) 12 (2022) 1196, https://doi.org/10.3390/diagnostics12051196.
[55] J.J. Cush, J.B. Splawski, R. Thomas, J.E. McFarlin, H. Schulze-Koops, L.S. Davis, K. Fujita, P.E. Lipsky, Elevated interleukin-10 levels in patients with rheumatoid arthritis, Arthritis Rheum. 38 (1995) 96–104, https://doi.org/10.1002/art.1780380115.
[56] C. Fiehn, M. Wermann, A. Pezzutto, M. Hüfner, B. Heilig, Plasma GM-CSF concentrations in rheumatoid arthritis, systemic lupus erythematosus and spondyloarthropathy, Z. Rheumatol. 51 (1992) 121–126.
[57] F.S. Frőschen, S. Schell, F.A. Schildberg, A. Klausing, H. Kohlhof, S. Gravius, T. M. Randau, Analysis of synovial biomarkers with a multiplex protein microarray in patients with PJI undergoing revision arthroplasty of the hip or knee joint, Arch. Orthop. Trauma Surg. 140 (2020) 1883–1890, https://doi.org/10.1007/s00402-020-03388-5.
[58] R.V. Lokhande, J.G. Ambekar, K.G. Bhat, N.N. Dongre, Interleukin-21 and its association with chronic periodontitis, J. Indian Soc. Periodontol. 23 (2019) 21–24, https://doi.org/10.4103/jisp.jisp_410_18.
[59] A. Jüngel, J.H. Distler, M. Kurowska-Stolarska, C.A. Seemayer, R. Seibl, A. Forster, B.A. Michel, R.E. Gay, F. Emmrich, S. Gay, O. Distler, Expression of interleukin-21 receptor, but not interleukin-21, in synovial fibroblasts and synovial macrophages of patients with rheumatoid arthritis, Arthritis Rheum. 50 (2004) 1468–1476, https://doi.org/10.1002/art.20218.
[60] Y. Okamatsu, D. Kim, R. Battaglino, H. Sasaki, U. Späte, P. Stashenko, MIP-1 gamma promotes receptor-activator-of-NF-kappa-B-ligand-induced osteoclast formation and survival, J. Immunol. 173 (2004) 2084–2090, https://doi.org/10.4049/jimmunol.173.3.2084.
[61] M. Yang, G. Mailhot, C.A. MacKay, A. Mason-Savas, J. Aubin, P.R. Odgren, Chemokine and chemokine receptor expression during colony stimulating factor-1-induced osteoclast differentiation in the toothless osteopetrotic rat: a key role for CCL9 (MIP-1 gamma) in osteoclastogenesis in vivo and in vitro, Blood 107 (2006) 2262–2270, https://doi.org/10.1182/blood-2005-08-3365.
[62] D. Varoga, M. Tohidnezhad, F. Paulsen, C.J. Wruck, L. Brandenburg, R. Mentlein, S. Lippross, J. Hassenpflug, L. Besch, M. Müller, C. Jürgens, A. Seekamp, L. Schmitt, T. Pufe, The role of human beta-defensin-2 in bone, J. Anat. 213 (2008) 749–757, https://doi.org/10.1111/j.1469-7580.2008.00992.x.
[63] D. Varoga, C.J. Wruck, M. Tohidnezhad, L. Brandenburg, F. Paulsen, R. Mentlein, A. Seekamp, L. Besch, T. Pufe, Osteoblasts participate in the innate immunity of the bone by producing human beta defensin-3, Histochem. Cell Biol. 131 (2009) 207–218, https://doi.org/10.1007/s00418-008-0522-8.
[64] F. Semple, J.R. Dorin, β-defensins: multifunctional modulators of infection, inflammation and more? J. Innate Immun. 4 (2012) 337–348, https://doi.org/10.1159/000336619.
[65] F. Semple, S. Webb, H.N. Li, H.B. Patel, M. Perretti, I.J. Jackson, M. Gray, D. J. Davidson, J.R. Dorin, Human beta-defensin 3 has immunosuppressive activity in vitro and in vivo, Eur. J. Immunol. 40 (2010) 1073–1078, https://doi.org/10.1002/eji.200940041.
[66] K.R. Parducho, B. Beadell, T.K. Ybarra, M. Bush, E. Escalera, A.T. Trejos, A. Chieng, M. Mendez, C. Anderson, H. Park, Y. Wang, W. Lu, E. Porter, The antimicrobial peptide human beta-defensin 2 inhibits biofilm production of Pseudomonas aeruginosa without compromising metabolic activity, Front. Immunol. 11 (2020) 805, https://doi.org/10.3389/fimmu.2020.00805.
[67] A.G. Hanan, A.S. Ahmed, Effect of β-defensin 2 on biofilm formation in pathogenic *E. coli* bacteria isolated from clinical samples, TJABS 4 (2022) 76–80.
[68] J. Harder, J. Bartels, E. Christophers, J.M. Schroder, Isolation and characterization of human beta -defensin-3, a novel human inducible peptide antibiotic, J. Biol. Chem. 276 (2001) 5707–5713, https://doi.org/10.1074/jbc.M008557200.
[69] D.M. Hoover, Z. Wu, K. Tucker, W. Lu, J. Lubkowski, Antimicrobial characterization of human β-defensin 3 derivatives, Antimicrob. Agents Chemother. 47 (2003) 2804–2809, https://doi.org/10.1128/AAC.47.9.2804-2809.2003.
[70] A. Matsugaki, M. Ito, Y. Kobayashi, T. Matsuzaka, R. Ozasa, T. Ishimoto, H. Takahashi, R. Watanabe, T. Inoue, K. Yokota, Y. Nakashima, T. Kaito, S. Okada, T. Hanawa, Y. Matsuyama, M. Matsumoto, H. Taneichi, T. Nakano, Innovative design of bone quality-targeted intervertebral spacer: accelerated functional fusion guiding oriented collagen and apatite microstructure without autologous bone graft, Spine J. 23 (2023) 609–620, https://doi.org/10.1016/j.spinee.2022.12.011.
[71] T. Ishimoto, K. Kawahara, A. Matsugaki, H. Kamioka, T. Nakano, Quantitative evaluation of osteocyte morphology and bone anisotropic extracellular matrix in rat femur, Calcif. Tissue Int. 109 (2021) 434–444, https://doi.org/10.1007/s00223-021-00852-1.
[72] R. Watanabe, A. Matsugaki, T. Ishimoto, R. Ozasa, T. Matsumoto, T. Nakano, A novel ex vivo bone culture model for regulation of collagen/apatite preferential orientation by mechanical loading, Int. J. Mol. Sci. 23 (2022) 7423, https://doi.org/10.3390/ijms23137423.
[73] B. Mirzashahi, M. Chehrassan, S.M.J. Mortazavi, Intrawound application of vancomycin changes the responsible germ in elective spine surgery without significant effect on the rate of infection: a randomized prospective study, Musculoskelet. Surg. 102 (2018) 35–39, https://doi.org/10.1007/s12306-017-0490-z.
[74] L. Pulido, E. Ghanem, A. Joshi, J.J. Purtill, J. Parvizi, Periprosthetic joint infection: the incidence, timing, and predisposing factors, Clin. Orthop. Relat. Res. 466 (2008) 1710–1715, https://doi.org/10.1007/s11999-008-0209-4.
[75] M.F. Chen, C.H. Chang, C.C. Hu, Y.Y. Wu, Y. Chang, S.W.N. Ueng, Periprosthetic joint infection caused by gram-positive versus gram-negative bacteria: lipopolysaccharide, but not lipoteichoic acid, exerts adverse osteoclast-mediated effects on the bone, J. Clin. Med. 8 (2019) 1289, https://doi.org/10.3390/jcm8091289.